High-Performance Transparent Conductive Films Using Rheologically Derived Reduced Graphene Oxide

Seung Yol Jeong,[†] Sung Hun Kim,[†] Joong Tark Han,[†] Hee Jin Jeong,[†] Sunhye Yang,[‡] and Geon-Woong Lee[†,*]

[†]Nano Carbon Materials Research Group and [‡]Battery Research Center, Korea Electrotechnology Research Institute, Changwon 641-120, Republic of Korea

ABSTRACT In this work, we produced large-area graphene oxide (GO) sheets with fewer defects on the basal plane by application of shear stress in solution to obtain high-quality reduced graphene oxide (RGO) sheets without the need for post-annealing processes. This is described as rheologically derived RGO. The large-area GO sheets were generated using a homogenizer in aqueous solution, which induced slippage of the GO in the in-plane direction during the exfoliation process, in contrast with the conventional sonication method. The effects of chemical reduction under mild conditions demonstrated that the formation of structural defects during the exfoliation process affected the RGO properties. In the Raman spectra, the I_D/I_G ratio of the homogenized RGO (HRGO) increased more than that of the sonicated RGO (SRGO) due to the large number of ordered six-fold rings on the basal plane. The enhanced sheet resistance of the HRGO thin film was found to be 2.2 kΩ/sq at 80% transmittance. The effective exfoliation method has great potential for application to high-performance RGO-transparent conducting films.

KEYWORDS: reduced graphene oxide · shear stress · homogenizer · exfoliation · structural defects · sheet resistance

Graphene has received great attention due to its superior electronic and mechanical properties, including high carrier mobility (200 000 $cm^2/(V \cdot s)$), thermal conductivity (~5000 W/mK), and Young's modulus (~1100 GPa).[1−4] Because of the 2D nature of graphene layers, it is also being considered as transparent conducting films (TCFs) and electronic devices due to the relative ease of control over the fabrication procedures and electronic structures in comparison with other carbon materials, such as carbon nanotubes and fullerene.[5] Several methods for producing graphene sheets, such as mechanical cleavage, epitaxial growth, chemical vapor deposition (CVD), and chemical exfoliation of graphite, have been introduced.[6−9]

Micromechanical exfoliation of graphite was exploited from Geim and co-workers at Manchester University, who introduced the well-known "Scotch tape" method.[6] This method is useful for fundamental studies and analysis of the intrinsic properties of a single-layered graphene. The remarkable transport properties of graphene present model systems for studying quantum Hall effects and massless Dirac fermions.[10] However, large-scale production of graphene has not been reliable due to low production yields. As a practical approach, graphene has been produced by a CVD method on metal substrates, such as Cu or Ni. The large-area electronics can be applicable by a contact printing method. Hong *et al.* at Sungkyunkwan University introduced an outstanding roll-to-roll production process for preparing graphene thin film with high performance.[11] Because the domains on a graphene sheet create defect sites during synthesis, the production of defect-free graphene sheets is still challenging. As a solution-based process, reduced graphene oxide (RGO) has been introduced, resulting from chemical exfoliation and reduction of graphite.[9] RGO is rendered with various stoichiometries and local arrangements of chemical functional groups, which can alter the intrinsic properties of the pristine graphene.[12] Although these drawbacks may hinder electrode or device performances, these two practical approaches are promising candidates for the large-area production of graphene sheets. In particular, the use of RGO can be efficiently applied in a straightforward manner to continuous process applications, for instance, screen printing, inkjet printing, or spray methods, *etc.*[13]

Several essential steps have been introduced into solution-based processes for the fabrication of RGO-TCFs: (i) chemical exfoliation and dispersion, (ii) chemical and thermal reduction, and (iii) transfer of large scalable RGO thin films. To date, GO has been generated by the chemical exfoliation of graphite by treatment with a strong acid as introduced by Hummers and Brodie.[14,15] This method yields hydroxyl and epoxy

*Address correspondence to gwleephd@keri.re.kr.

Received for review August 13, 2010 and accepted January 12, 2011.

Published online January 24, 2011
10.1021/nn102017f

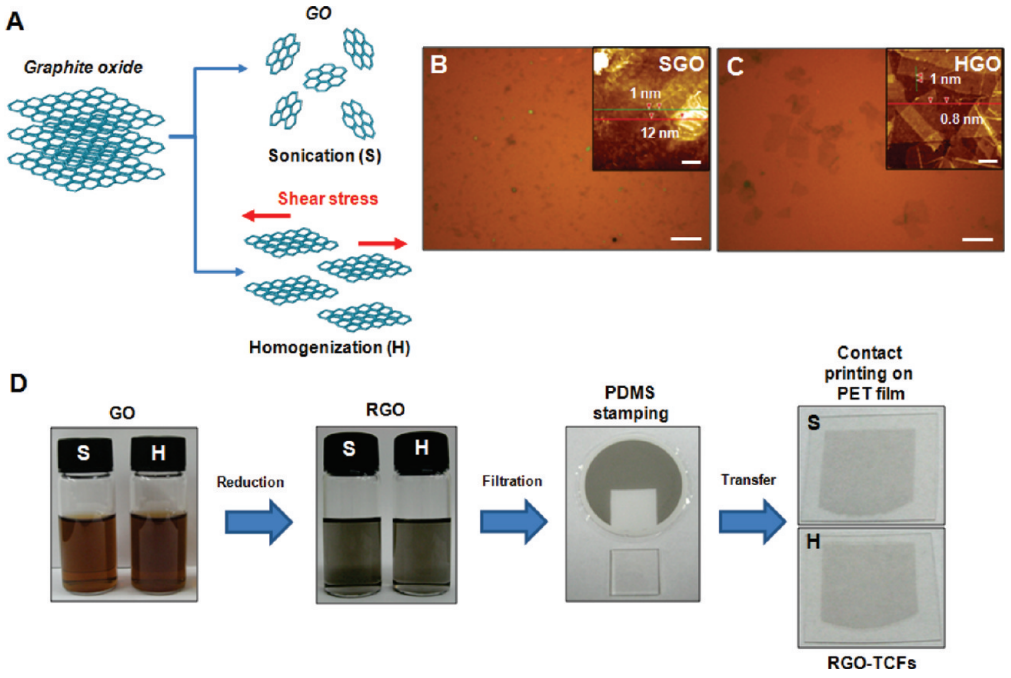

Figure 1. Production of GO and RGO sheets by two types of exfoliation methods. (A) Schematic diagram for the exfoliation mechanism of GO *via* sonication (S) or homogenization (H). (B,C) Optical images of the sonicated and homogenized GO samples on a 300 nm thick SiO_2 substrate (inset: AFM images of the GO sheets). (D) Experimental procedure for the fabrication of RGO-TCFs by the contact printing method. The scale bars in (B) and (C) are 10 μm, and those in the two insets are 2 μm.

groups in the basal plane and carbonyl and carboxyl groups on the edge sites.[16] The hydrophilic functional groups facilitate exfoliation and dispersion of GO in aqueous solutions with sonication, although large numbers of structural defects and oxygen functional groups with insulating properties are also present. To improve the electrical performance, subsequent reduction processes are necessary to remove the oxygen moieties. Ultracentrifugation and graphite exfoliation without acid treatment have been reported to retain the intrinsic properties of graphene with superior electrical properties.[17] Preparation methods for high-quality graphene sheets without oxygen functional groups have been investigated. However, low yields of graphene sheets were obtained in these cases. Another approach to the production of large scalable graphene sheets involved chemical reduction treatment, and the resultant sheets were described as chemically derived reduced graphene (CDG).[18] The widely used reduction processes include exposure to hydrazine vapor and thermal annealing at high temperatures to enhance the electrical conductivity. Although various reduction processes have been reported, obtaining high-performance optoelectrical properties from RGO-TCFs remains a challenge due to the large number of structural defects and residual oxygen functional groups in RGO sheets.

Here, we describe a novel method that is suitable for production of large-area and high-performance RGO thin films. On the basis of the concept of the 2D nature of graphene, this method was exploited for the formation of GO sheets by control of exfoliation in solution. Significantly, GO sheets with much larger areas than those produced by conventional sonication methods were obtained using a homogenizer, which applied a shear-induced exfoliation mechanism. The GO sheets were then reduced by hydrazine in organic solvents. The produced RGO sheets are described as a rheologically derived RGO. This method is easy and straightforward to implement the production of large-area RGO sheets with fewer defects. Intriguingly, the differences of Raman spectra between the sonicated RGO (SRGO) and homogenized RGO (HRGO) demonstrated an unprecedented extent of reduction due to the structural defects of the GO on the basal plane, which influenced the sp^3 bonds and oxygen functional groups. This emphasized that the formation of structural defects, the reduction of oxygen functional groups, and the size of RGO sheets were affected by exfoliated GO through rheological engineering. This is applicable for high-performance TCFs and electronic devices.

RESULTS AND DISCUSSION

Production of Large Area RGO Sheets by Induced Shear Stress. We prepared single-layered graphene oxide by the modified Brodie method.[14] Briefly, pure graphite (average size is 70 μm from natural graphite powder, Alfar Aesar, 99.999% purity, −200 mesh) was treated with fuming nitric acid and sodium chlorate at room temperature with stirring for 48 h. In general, graphite oxide reveals an expanded interlayer spacing from

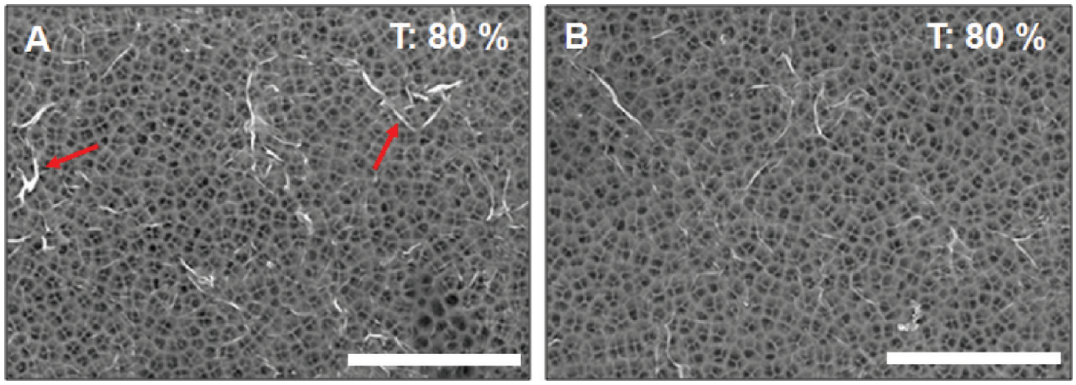

Figure 2. FE-SEM images of (A) SRGO and (B) HRGO thin films on an AAO filter with 80% transmittance (scale bars are 2 μm.).

0.34 nm (pure graphite) to >0.6 nm (graphite oxide) due to the oxygen functional groups, thus, exfoliation is activated by the weakening of van der Waals forces between layers.[19] The GO solution was prepared using two exfoliation methods that employed either a homogenizer (H) or a sonicator (S), as described in the schematics of Figure 1A. Due to the 2D morphologies of GO, the homogenizer process promoted the nondestructive exfoliation of graphite oxide because slippage of the GO was induced in the in-plane direction by shear stress, which was described as a rheologically derived GO. The conventional bath sonicator vigorously destroyed the pristine structure of the GO, thereby producing a small size due to acoustical wave agitation in solution. Significantly, the atomic force microscope (AFM) images of GO sheets on a 300 nm SiO_2 substrate revealed that the average thickness was about 1 nm in both cases, as shown in the inset of Figure 1B,C. The average size of sonicated GO (SGO) sheets (a few square micrometers) was smaller than that of the homogenized GO (HGO) sheets (a few hundred square micrometers) in the optical images of Figure 1B,C. The SGO exhibited some agglomerated GO on the silicon substrate due to the small size distribution of the sheets. In previous reports, the large-area GO sheets were obtained by a stepwise centrifugation method and addition of surfactants with the use of a conventional sonication process and the large size of graphite powder (700 μm to 5 mm).[20,21] The size distribution of GO sheets was from a few hundred square micrometers to square millimeters, depending on the condition of centrifugation. To confirm the exfoliation effect of GO sheets between HGO and SGO, we carried out the homogeneous dispersion of GO sheets in aqueous solution without the additional process of using a small size of graphite powder (70 μm). The rheologically derived or sonicated exfoliation and dispersion of GO sheets was accomplished (Figure 1D) by homogeneously dispersing from the synthesized graphite oxide using H or S in an aqueous NaOH solution at pH 10 for 1 h. The prepared GO solutions were then diluted in dimethylformamide (DMF) to a concentration of 90 wt %, and then we performed the hydrazine reduction for the RGO formation. The effects of hydrazine reduction conditions on HGO and SGO were compared as a function of the reducing agent concentration and temperature. Aqueous hydrazine monohydrate (N_2H_4) was dropped into the diluted GO solutions with stirring at a concentration of 0.4 mM at 50 °C (condition I), 4 mM at 50 °C (condition II), and 4 mM at 80 °C (condition III) for 16 h. The final products were labeled HRGO and SRGO in this work. The film was prepared by the filtration method over anodic aluminum oxide (AAO) and washed with DMF solvent. Figure 2 shows that the filtered SRGO and HRGO sheets were uniformly coated on the AAO surface. However, as indicated by the red arrows in Figure 2A, the SRGO film revealed more agglomeration than the HRGO film due to the small size sheet, which is described in Figure 1B,C. Subsequently, the films were transferred to a PET film by the contact printing method with PDMS stamping. The sheet resistances (R_{sh}) of the transferred RGO films were consistent with the properties of the filtrated film on the AAO filter, as confirmed by four-probe measurements. The optoelectrical characteristics of the HRGO and SRGO thin films exhibited different transport phenomena under mild hydrazine reduction condition I (0.4 mM N_2H_4, 50 °C). The R_{sh} of HRGO-I was about 10 times lower than that of SRGO-I, which was found to be 5 and 49 kΩ/sq at transmittance (T) = 80%, as shown in Figure 5A. The enhanced HRGO thin films yielded an R_{sh} of 2.2 kΩ/sq under condition III (4 mM N_2H_4, 80 °C). This method is easy and straightforward for fabrication of high-performance and large-area RGO-TCFs.

Enhanced Characteristics of the HRGO and Comparison with the SRGO Thin Films. Raman analysis provides further insight into the number of layers, doping, and structural changes of the RGO in terms of GO dispersion and exfoliation, as shown in Figure 3. The second-order zone boundary phonon (2D) peaks were monitored at 2649 and 2646 cm^{-1} with a symmetric line shape, without the presence of shoulder peaks for the SRGO and HRGO, respectively, confirming a single-layered graphene in Figure 3A,B.[22] However, the 2D intensity was still lower than that of CVD-grown graphene due to the presence of residual oxygen functional groups.[8] As a consistent result from AFM images in the insets of

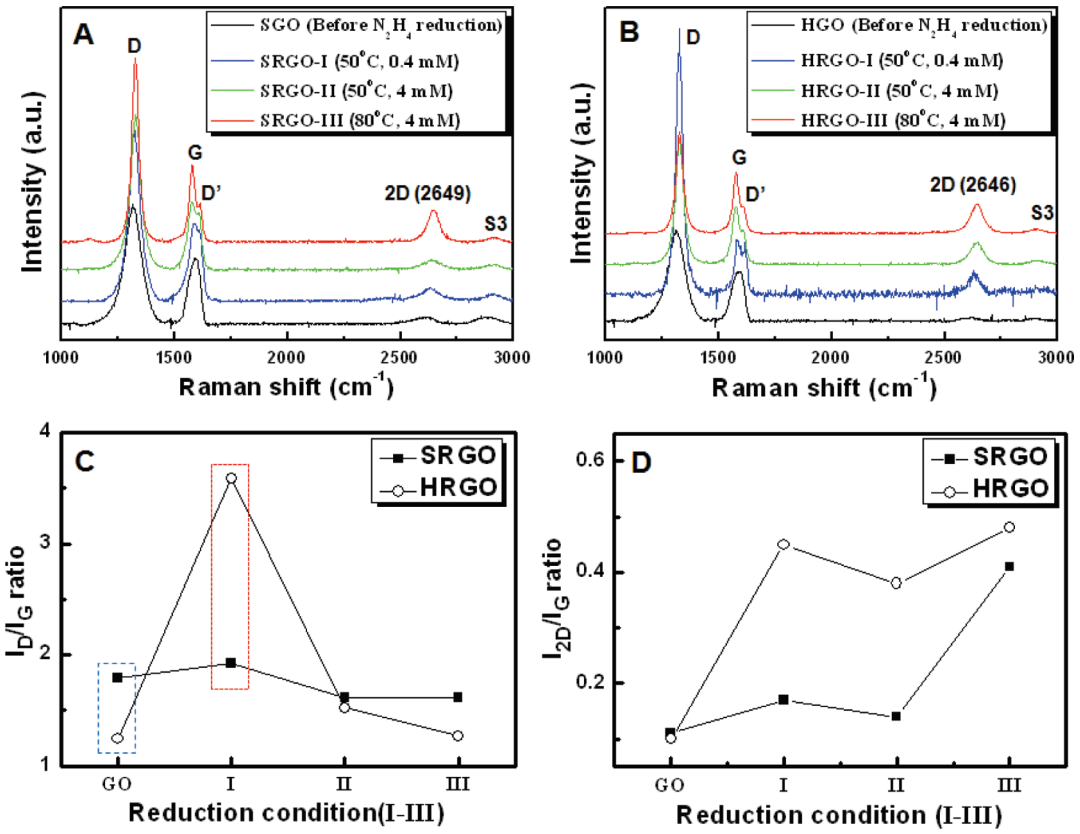

Figure 3. Raman spectra of (A) SRGO and (B) HRGO depending on the mild hydrazine reduction conditions: (I) a reduction temperature of 50 °C with 0.4 mM N_2H_4; (II) 50 °C, 4 mM N_2H_4; (III) 80 °C, 4 mM N_2H_4. (C,D) Areal intensity ratios of I_D/I_G and I_{2D}/I_G as a function of the reduction conditions from I to III (blue dashed square, S- and HGO; red dashed square, S- and HRGO-I).

Figure 1B,C, the thicknesses of the RGO layers were about 0.8−1 nm. The structural changes on the basal plane of GO sheets, such as imperfections, were measured by Raman spectroscopy with the laser spot size of 1 μm. These were characterized by reducing the oxygen moieties in SRGO and HRGO by hydrazine reduction under mild conditions I−III because the reduction ratio did not alter under severe reduction conditions. The mild conditions varied with respect to the concentration of reducing agent (0.4 or 4 mM) and reaction temperature (50 or 80 °C). Before hydrazine reduction, as indicated by the blue dashed square in Figure 3C, the I_D/I_G ratio of SGO was higher than that of HGO. In amorphous carbon states, the strength of the D peak is proportional to an average interdefect distance (L_a), indicating that a higher defect density has a smaller L_a.[23] The defects were mainly created by mechanical forces through the exfoliation process and by chemical interaction of oxygen moieties. Although the defect density owing to the mechanical force was higher in the SGO than in the HGO (this can be proved by an average sheet size of both samples as shown in AFM images of Figure 1), the total structural defect density of the HGO was higher than the SGO because the abundant defects were formed by the chemical interaction in the HGO. The XPS revealed that the atomic percentage of oxygen functional groups on the basal plane of HGO, such as sp^3, epoxy, and hydroxyl groups, was much higher than that of the SGO, as shown in Table 1. In Raman spectra, it was mostly acquired from the basal plane of the S/HGO samples, thus the defects were dominantly reflected by the chemical interaction of oxygen moieties. In this case, the HGO had a smaller L_a than that of the SGO. Substantially, the structural defects by chemical interaction demonstrated by mild hydrazine reduction that the sudden change of I_D/I_G ratio for the HRGO-I (large L_a) compared to the SRGO-I (small L_a) was caused by the decrease of oxygen functional groups. After mild hydrazine reduction with condition (I: 0.4 mM, 50 °C), indicated by the red dashed square in Figure 3C, the I_D/I_G ratio of S/HRGO-I increased by reduction of the oxygen moieties. The defect (D) peak arises from the intervalley scattering due to the large amount of smaller graphene domains on the basal plane, which indicated a phonon confinement.[23,24] In particular, the I_D/I_G ratio of HRGO-I was significantly higher than that of the SRGO-I. The differences in the I_D/I_G ratio under mild conditions provided information on the basal plane of RGO sheets about the structural defects, including the effects of exfoliation and chemical reduction.[25] In case of the sp^2 and sp^3 amorphous carbon states, the structural defects consisted of ordered hexagonal six-fold rings and other disorders, such as heptagon and pentagon rings,

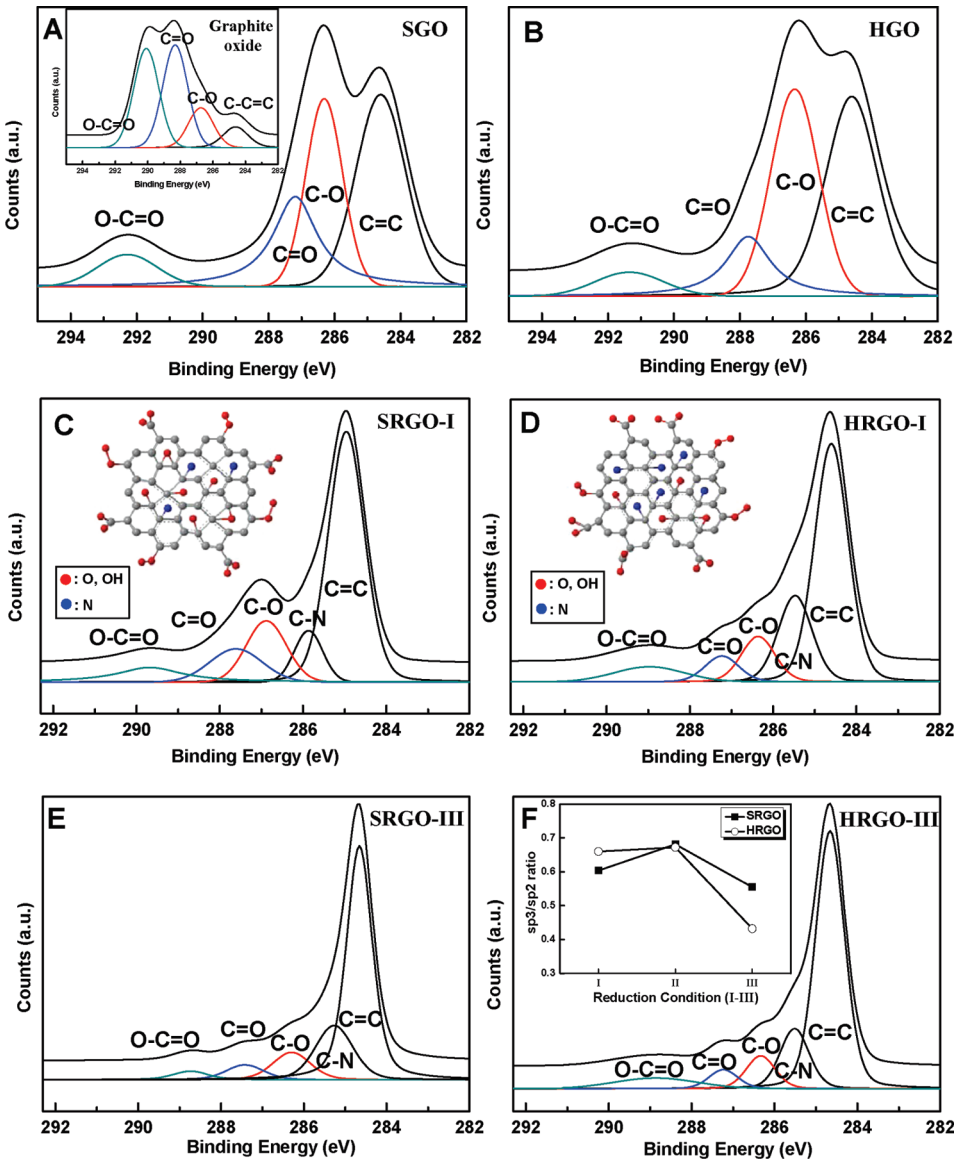

Figure 4. XPS analysis of the hydrazine reduction products SRGO and HRGO with deconvolution by peak fitting. Before hydrazine reduction of (A) SGO (inset: graphite oxide powder) and (B) HGO, the RGO produced by the three hydrazine reduction conditions from I to III: (C) SRGO-I (inset: schematic diagram of SRGO with structural defects on the basal plane), (D) HRGO-I (inset: HRGO with the formation of ordered six-fold rings on the basal plane), (E) SRGO-III, and (F) HRGO-III (inset: differences in the sp^3/sp^2 carbon ratio as a function of hydrazine reduction conditions from I to III).

as described in the insets of Figure 4C,D. The strength of the D peak depended on the probability of finding a six-fold ring in the cluster, thus, the development of a D peak indicated ordering among the amorphous carbons.[26,27] Therefore, the distribution of ordered six-fold rings on the HRGO-I was higher than that of SRGO-I due to fewer defects in the HGO with large L_a during the exfoliation process, as shown by the blue dashed square in Figure 3C. It also has a strong correlation that the I_{2D}/I_G ratio of HRGO-I was higher than that of SRGO-I, as shown in Figure 3D. The intensities of the second-order Raman peaks (2D) were sensitive to the ordering structures on the basal plane of the graphene. These peaks detected changes not only in the polarizability but also in the symmetric and asymmetric vibrational energies. Thus, the broadened fwhm and weak intensity of 2D peaks indicated the disordered carbon ring structures on the basal plane of the graphene.[28,29] Moreover, the increase of the I_{2D}/I_G ratio may have been governed by the dedoping of holes as a result of phonon softening by deoxygenation of the graphene.[30] These data agree with the finding of the X-ray photoelectron spectroscopy (XPS) analysis that a relatively low atomic percentage of epoxy and hydroxyl groups and a high percentage of sp^3 region was present on the basal plane in HRGO-I, as shown in Figure 4C,D. Additionally, the R_{sh} of HRGO-I (5 kΩ/sq) was 10 times lower than that of SRGO-I (49 kΩ/sq) at 80% transmittance, indicated by the red dashed circle of Figure 5A. High-performance RGO sheets were obtained by

TABLE 1. Analysis of C1s Peak Positions and the Relative Atomic Percentages of sp^2, sp^3, and Oxygen Functional Groups with Respect to Pristine Graphite Oxide, Before Hydrazine Reduction, S/HGO, and after Hydrazine Reduction, S/HRGO, as a Function of Hydrazine Reduction Conditions From I to III

	C=C	C−C/C−N	C−O	C=O	COOH
graphite oxide	284.6(8.53%)		286.7(15.0%)	288.3(38.9%)	290.1(37.6%)
SGO	284.6(39.8%)		286.3(28.2%)	287.2(24.2%)	292.3(7.8%)
HGO	284.6(43.27%)		286.3(36.1%)	287.7(14.6%)	291.3(6.1%)
SRGO-I	284.6(57.6%)	285.5(8.7%)	286.5(15.7%)	287.2(10.4%)	289.3(8.6%)
HRGO-I	284.6(56.1%)	285.4(20.3%)	286.4(10.7%)	287.5(6.0%)	289.4(6.8%)
SRGO-II	284.6(56.4%)	285.4(21.8%)	286.8(11.5%)	288.0(5.1%)	289.7(5.1%)
HRGO-II	284.6(56.7%)	285.4(23.1%)	286.5(9.1%)	287.8(5.1%)	289.6(6.6%)
SRGO-III	284.6(62.3%)	285.3(19.5%)	286.3(9.8%)	287.4(5.3%)	289.1(3.1%)
HRGO-III	284.6(64.8%)	285.5(15.1%)	286.3(8.2%)	287.2(4.7%)	289.0(7.1%)

performing the reaction under more severe conditions, II and III, at 50 and 80 °C, respectively, in the presence of 4 mM N_2H_4. However, the deviation of I_{2D}/I_G ratio between HRGO and SRGO at the reduction condition III ($\Delta I_{2D}/I_G = 0.1$) was lower than that of conditions I (0.28) and II (0.24) due to intensive reduction on the RGO sheets, as shown in Figure 3D. Although it revealed the decreased deviation, the carrier mobility increased more than 2 times as the I_{2D}/I_G ratio increased by about 0.1.[31] In Figure 3C, the I_D/I_G ratios of HRGO-III (large L_a) were lower than those of SRGO-III (small L_a), indicating an inverse proportionality relationship between I_D/I_G ratio and the average size of sp^2 domains due to formation of crystalline structures in the graphene.[23,27] These results demonstrate that low defect formation on the basal plane of the GO sheets, *via* the highly effective exfoliation process, is a prerequisite for the production of high-performance RGO-TCFs.

XPS also revealed different degree of oxygen functional group loss in HRGO and SRGO conditions. The inset of Figure 4A shows the C1s peak of graphite oxide, which consists of four typical components arising from C=C/C−C (sp^2 and sp^3, ~284.6 eV), C−O (hydroxyl and epoxy, ~286.7 eV), C=O (carbonyl, ~288.3 eV), and O−C=O (carboxyl, 290.1 eV) as described previously.[32] Subsequent to exfoliation and dispersion in NaOH solution at pH 10 to enhance the dispersibility of the GO sheets in DI water,[33] the presence of the carbonyl and carboxyl groups in S- and HGO decreased dramatically, which was attributed to the mildly alkaline reduction conditions, despite the low concentration of NaOH in solution.[34] In contrast, the epoxy and hydroxyl groups relatively increased due to formation of the GO layers by exfoliation of graphite oxide, as shown in Figure 4A,B. The atomic percentages of C=C−C and C−O bonds in the HGO were higher than that in the SGO. This indicated that the HGO sheets formed with a large area and fewer structural defects compared to the SGO sheets, in agreement with the optical images and I_D/I_G ratio from the Raman spectra in Figures 1C and 3C. Although the carboxyl and carbonyl groups of S- and HGO decreased, these RGO sheets exhibited an insulating behavior according to the R_{sh} measurement. This suggested that the electrical conductivity of the RGO sheets was dominantly affected by the oxygen functional groups on the basal plane. In changing reduction conditions from I to III, the sp^2 atomic ratio increased slightly with the S- and HRGO, as indicated in Table 1. It should be noted that compared to conditions investigated previously, the conditions used in the present work were not as harsh, involving lower quantities of hydrazine and lower temperatures. Figure 4C,D presents the different degrees of functional group loss under the hydrazine reduction condition I. The total areal intensity of the oxygen functional groups, including hydroxyl, epoxy, carbonyl, and carboxyl groups on the HRGO-I, was lower than on the SRGO-I. In particular, the sp^3 (C−N bond) content of HRGO-I (20.3%) was intensively higher than that of SRGO-I (8.7%), whereas the sp^2 atomic percentages were similar regardless of the equivalency of the reduction rates in both cases. The sp^3 bonds on the basal plane were present in the ordered six-fold and disordered carbon rings. The SRGO layers were produced by sonication and displayed carbon rings that were more disordered than those of HRGO. Thus, the probability of finding the ordered six-fold rings in HRGO-I was relatively higher than in SRGO-I.[23,26] The schematic diagrams in the insets of Figure 4C,D describe that the sp^3, epoxy, and hydroxyl groups on RGO were affected by the structural defects created during the exfoliation process of the GO formation. In reasonable agreement, the sp^3/sp^2 carbon ratio determined by the XPS spectra corresponded to the I_D/I_G ratio in the Raman spectra, as shown in the inset of Figure 4F. Therefore, the structural defects on the basal plane of GO were directly affected by the exfoliation procedure. This observation agreed with the lower R_{sh} for HRGO-I than for SRGO-I at 80% transmittance, indicated by the red dashed circle of Figure 5A. This approach highlights two substantial issues for the formation of effective RGO: (i) large-area GO sheets by shear stress effects produced larger basal planes, and (ii) the formation of structural defects during the exfoliation process was a crucial factor for high-performance RGO engineering, in strong correlation

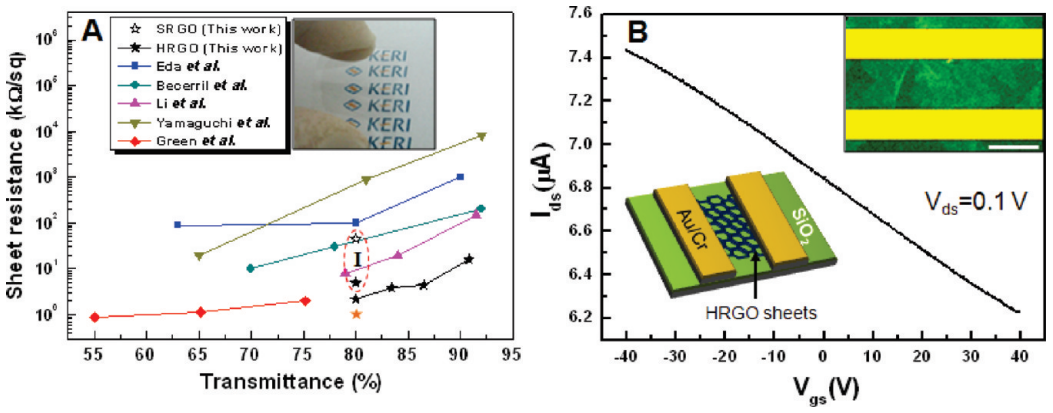

Figure 5. Optoelectrical and electrical properties RGO thin films. (A) Sheet resistance *vs* transmittance of RGO-TCFs under reduction condition III from previously reported results and our work; the filled stars indicate our data for the HRGO (red dashed circle, comparison of R_{sh} of HRGO (filled star) and SRGO (open star) at T = 80% under reduction condition I; yellow star, the R_{sh} of HRGO-III thin film was 750 Ω/sq at T = 80% with Au ion doping). (B) $I_{ds}-V_{gs}$ characteristics of the HRGO-III film in the gate bias range from −40 to 40 V (inset: optical image (upper right), and schematic diagram of HRGO-TFT).

with the optical images and I_D/I_G ratio from the Raman spectra shown in Figures 1C and 3C. As the hydrazine concentration increased from reduction conditions II and III, the sp^2 atomic percentages increased as the presence of other oxygen functional groups decreased. In condition II, the sp^3 region increased much more than in the other conditions, due to 10-fold higher concentration of hydrazine reducing agent without changes in temperature, as shown in Table 1. Figure 4E,F reveals that the difference in areal intensity of the oxygen functional groups in the SRGO-III and HRGO-III was not significant. Although the atomic ratios of the oxygen functional groups on the RGO were similar both cases, the extent of defect formations on the basal plane was lower than in SRGO, as described by the Raman spectra shown in Figure 3C. These results suggest that the formation of GO sheets by shear stress can significantly influence not only the low defect formation on the basal plane but also the performance of large-area RGO sheets.

Figure 5A shows the sheet resistance (R_{sh}) *versus* transmittance depending on the HRGO films. Under reduction condition I, as indicated by the red dashed circle of Figure 5A, the R_{sh} of HRGO-I (filled star) was 10 times lower than that of SRGO-I (empty star), corresponding to 5 and 49 kΩ/sq, respectively, at T = 80%. This result demonstrated that the large-area and high-quality RGO sheets influenced the R_{sh} of thin films because the series resistance, including contact and RGO sheet resistances, depended on the size distribution, residual oxygen moieties, and presence of defects on the RGO sheets. In the case of higher-performance HRGO thin films produced under the reduction condition III, the R_{sh} values were less than those of condition I, which exhibited 2.2 kΩ/sq at 80% transmittance. These results are comparable to the values reported by others in studies of the optoelectrical properties of RGO using hydrazine reduction.[17,31,35−37] Although the hydrazine reduction conditions without a post-annealing step were mild, the R_{sh} values of our HRGO films were much smaller than those of other recent works, in strong agreement with the Raman and XPS results. However, HRGO-III yielded a higher R_{sh} than CVD-grown graphene due to residual oxygen moieties and the incomplete restoration of crystallinity. To enhance the electrical properties, the HRGO-III was selected for doping with $HAuCl_4$. The R_{sh} consistently decreased by 30% at T = 80%, as shown by the yellow star of Figure 5A. The Au ions acted as electron-withdrawing groups, thus increasing the hole carrier concentration, similar to the effects observed for carbon nanotube doping.[38] To verify the high conductivity of the HRGO-III sheets, the carrier mobility was measured, as described in Figure 5B. The inset of Figure 5B shows a fabricated HRGO thin film transistor (HRGO-TFT). The metal electrodes were fabricated by conventional photolithography. The device showed typical p-type behavior in ambient conditions due to adsorbates comprising oxygen moieties. The $I_{ds}-V_{gs}$ curve was observed over the range of −40 to 40 V gate voltages with a constant V_{ds} of 0.1 V. The hole carrier mobility was calculated from the linear region of the $I_{ds}-V_{gs}$ curves using the following equation:[31]

$$\mu_h = Lg_m/WC_0V_{ds}$$

where μ_h is hole mobility, L and W are channel length and width, g_m (dI_{ds}/dV_{gs}) is transconductance, C_0 is capacitance for 300 nm thick silicon oxide, and V_{ds} is the drain−source voltage (0.1 V). In previous characterizations of chemically derived RGO, the hole mobility was reported to be about 0.01−1 $cm^2/(V\cdot s)$. Recently, solvothermal reduction treatment at 180 °C yielded hole mobilities of 10−30 $cm^2/(V\cdot s)$.[24] In our work, the HRGO-TFT had substantially higher hole mobility (95 $cm^2/(V\cdot s)$) than that of other works using the sonication method. Significantly, the strong correlation between the Raman and XPS spectra demonstrated that the rheologically derived large-area GO

sheets efficiently minimized the formation of structural defects on the basal plane of the RGO sheets, yielding higher performance.

CONCLUSIONS

We have produced rheologically derived RGO sheets by inducing shear stress using a homogenizer. Large-area GO sheets were obtained by this modified exfoliation and dispersion process in higher yields than can be achieved using a conventional sonication method. The shear-induced exfoliation process for preparing GO significantly influenced RGO formation, not only by introducing fewer structural defects on the basal plane but also by producing large-area RGO sheets with high quality. The proposed approach is straightforward and enables the practical use of high-performance large-area RGO thin films, such as TCFs and electronic devices.

METHODS

Graphite oxide was synthesized using a modified Brodie method.[14] Pure graphite (Alfar Aesar, 99.999% purity, −200 mesh) was mixed with fuming nitric acid and sodium chlorate at room temperature with stirring for 48 h. Subsequent to the acid treatment, the purification process was carried out by washing, filtering, and cleaning. The GO solution was prepared *via* two exfoliation and dispersion processes as described in the schematics of Figure 1A. The synthesized graphite oxide was immersed in an aqueous NaOH solution at pH 10 with a concentration of 100 mg/L, then exfoliation and dispersion were carried out using either a homogenizer (H) or sonicator (S) for 1 h. The GO was exfoliated and dispersed in the solution homogeneously at 10 000 rpm in the homogenizer, and the power level of the conventional bath sonicator was 150 W. The prepared GO solutions were then diluted in dimethylformamide (DMF) to a concentration of 90 wt %, with respect to the dispersion of RGO after hydrazine reduction. The effects of hydrazine reduction conditions under H or S were tested as a function of reducing agent concentration and temperature. Aqueous hydrazine monohydrate (N_2H_4) was added dropwise to the diluted GO solutions to a final concentration of 0.4 or 4 mM, followed by heating at 50 or 80 °C for 16 h, respectively. Films were formed by filtration using anodic aluminum oxide (AAO) as shown in Figure 2. After washing, the RGO was transferred to a PET film by the contact printing method using PDMS stamping. To enhance the HRGO-TCFs performance, 20 μM aqueous $HAuCl_4$ was spin-coated onto the HRGO film at 2500 rpm for 1 min.

The absorbance properties of prepared GO and RGO solutions were measured by absorption spectroscopy (using a Varian Cary winRV). The morphologies of SRGO and HRGO were imaged by optical microscopy (Nikon Eclipse LV100), atomic force microscopy (AFM, Park Systems XE-100 Multimodes), and field emission scanning electron microscopy (FE-SEM, HITACHI S4800). The structural characteristics of the RGO sheets were investigated by a high-resolution Raman spectrometer (LabRAM HR 800 UV) with an excitation wavelength of 633 nm (1.96 eV) and a Rayleigh line injection filter with a spectral range of 100−3600 cm^{-1} to account for the Stokes shift. To confirm the change in the carbon to oxygen atomic ratio in the functional groups of the H and S samples after reduction, the X-ray photoelectron spectroscopy (XPS) analysis was carried out using a Multilab2000 (Thermo VG Scientific Inc.) spectrometer with monochromatized Al Kα X-ray radiation as the X-ray excitation source. The power was set to 150 W and the voltage to 20 eV for high-resolution scanning, and a 500 μm diameter beam size was used. The fitted peaks of XPS spectra were determined by considering a combination of Gaussian and Lorentzian distributions. To identify the optoelectrical characteristics of the HRGO and SRGO samples, the sheet resistance and transmittance were measured using a four-probe tester (Loresta, MCP-T610) and an absorption spectrometer. The $I_{ds}-V_{gs}$ measurement was performed by two-probe measurement to characterize the carrier mobility and type of HRGO in ambient condition. The supernatant HRGO solution was dropped onto a 300 nm thick SiO_2 substrate. The electrode pattern was obtained using conventional photolithography process. The channel width and length of metal electrode was 10 and 150 μm. The Cr and Au electrodes were deposited using a thermal evaporator at 2×10^{-6} Torr to a thickness of 20 and 100 nm, respectively.

Acknowledgment. This study was supported by funding from KERI(Grant 11-12-N0101-45).

REFERENCES AND NOTES

1. Novoselov, K. S.; Geim, A. K.; Morozov, S. V.; Jiang, D.; Katsnelson, M. I.; Grigorieva, I. V.; Dubonos, S. V.; Firsov, A. A. Two-Dimensional Gas of Massless Dirac Fermions in Graphene. *Nature* **2005,** *438*, 197–200.
2. Lee, C.; Wei, X.; Kysar, J. W.; Hone, J. Measurement of the Elastic Properties and Intrinsic Strength of Monolayer Graphene. *Science* **2008,** *321*, 385–388.
3. Balandin, A. A.; Ghosh, S.; Bao, W.; Calizo, I.; Teweldebrhan, D.; Mial, F.; Lau, C. N. Superior Thermal Conductivity of Single-Layer Graphene. *Nano Lett.* **2008,** *8*, 902–907.
4. Bolotin, K. I.; Sikes, K. J.; Jiang, Z.; Klima, M.; Fudenberg, G.; Hone, J.; Kim, P.; Stormer, H. L. Ultrahigh Electron Mobility in Suspended Graphene. *Solid State Commun.* **2008,** *146*, 351–355.
5. Compton, O. C.; Nguyen, S. T. Graphene Oxide, Highly Reduced Graphene Oxide, and Graphene: Versatile Building Blocks for Carbon-Based Materials. *Small* **2010,** *6*, 711–723.
6. Novoselov, K. S.; Geim, A. K.; Morozov, S. V.; Jiang, D.; Zhang, Y.; Dubonos, S. V.; Grigorieva, I. V.; Firsov, A. A. Electric Field Effect in Atomically Thin Carbon Films. *Science* **2004,** *306*, 666–669.
7. Berger, C.; Song, Z. M.; Li, X. B.; Wu, X. S.; Brown, N.; Naud, C.; Mayou, D.; Li, T. B.; Hass, J.; Marchenkov, A. N.; Conrad, E. H.; First, P. N.; de Heer, W. A. Electronic Confinement and Coherence in Patterned Epitaxial Graphene. *Science* **2006,** *312*, 1191–1196.
8. Kim, K. S.; Zhao, Y.; Jang, H.; Lee, S. Y.; Kim, J. M.; Kim., K. S.; Ahn, J.; Kim, P.; Choi, J.; Hong, B. H. Large-Scale Pattern Growth of Graphene Films for Stretchable Transparent Electrodes. *Nature* **2009,** *457*, 706–710.
9. Stankovich, S.; Dikin, D. A.; Dommett, G. H. B.; Kohlhaas, K. M.; Zimney, E. J.; Stach, E. A.; Piner, R. D.; Nguyen, S. T.; Ruoff, R. S. Graphene-Based Composite Materials. *Nature* **2006,** *442*, 282–286.
10. Zhang, Y. B.; Tan, Y. W.; Stormer, H. L.; Kim, P. Experimental Observation of the Quantum Hall Effect and Berry's Phase in Graphene. *Nature* **2005,** *438*, 201–204.
11. Bae, S.; Kim, H.; Lee, Y.; Xu, X.; Park, J.; Zheng, Y.; Balakrishnan, H.; Lei, T.; Kim, H. R.; Song, Y. I.; Kim, Y.; Kim, K. S.; Ozyilmas, B.; Ahn, J.; Hong, B. H.; Iigima, S. Roll-to-Roll Production of 30-in. Graphene Films for Transparent Electrodes. *Nat. Nanotechnol.* **2010,** *5*, 574–578.
12. Stankovich, S.; Piner, R. D.; Chen, X. Q.; Wu, N. Q.; Nguyen, S. T.; Ruoff, R. S. Stable Aqueous Dispersions of Graphitic Nanoplatelets *via* the Reduction of Exfoliated Graphite Oxide in the Presence of Poly(sodium 4-styrenesulfonate). *J. Mater. Chem.* **2006,** *16*, 155–158.

13. Gilje, S.; Han, S.; Wang, M.; Wang, K. L.; Kaner, R. B. A Chemical Route to Graphene for Device Applications. *Nano Lett.* **2007,** *7*, 3394–3398.
14. Brodie, B. C. Sur le poids atomique du graphite. *Ann. Chim. Phys.* **1860,** *59*, 466–472.
15. William, J.; Hummers, R. E.; Offeman, J. Preparation of Graphitic Oxide. *J. Am. Chem. Soc.* **1958,** *80*, 1339.
16. Li, X.; Zhu, Y.; Cai, W.; Borysiak, M.; Han, B.; Chen, D.; Piner, R. D.; Colombo, L.; Ruoff, R. S. Transfer of Large-Area Graphene Films for High-Performance Transparent Conductive Electrodes. *Nano Lett.* **2009,** *9*, 4359–4363.
17. Green, A. A.; Hersam, M. C. Solution Phase Production of Graphene with Controlled Thickness *via* Density Differentiation. *Nano Lett.* **2009,** *9*, 4031–4036.
18. Eda, G.; Chhowalla, M. Chemically Derived Graphene Oxide: Towards Large-Area Thin-Film Electronics and Optoelectronics. *Adv. Mater.* **2010,** *22*, 1–24.
19. Si, Y.; Samulski, E. T. Synthesis of Water Soluble Graphene. *Nano Lett.* **2008,** *8*, 1679–1682.
20. Zhao, J.; Pei, S.; Ren, W.; Gao, L.; Cheng, H. Efficient Preparation of Large-Area Graphene Oxide Sheets for Transparent Conductive Films. *ACS Nano* **2010,** *4*, 5245–5252.
21. Zhou, X.; Liu, Z. A Scale, Solution-Phase Processing Route to Graphene Oxide and Graphene Ultralarge Sheets. *Chem. Commun.* **2010,** *46*, 2611–2613.
22. Ferrari, A. C.; Meyer, J. C.; Scardaci, V.; Casiraghi, C.; Lazzeri, M.; Mauri, F.; Piscanec, S.; Jiang, D.; Novoselov, K. S.; Roth, S.; Geim, A. K. Raman Spectrum of Graphene and Graphene Layers. *Phys. Rev. Lett.* **2006,** *97*, 187401.
23. Ferrari, A. C. Raman Spectroscopy of Graphene and Graphite: Disorder, Electron−Phonon Coupling, Doping, and Nonadiabatic Effects. *Solid State Commun.* **2007,** *143*, 47–57.
24. Wang, H.; Robinson, J. T.; Li, X.; Dai, H. Solvothermal Reduction of Chemically Exfoliated Graphene Sheets. *J. Am. Chem. Soc.* **2009,** *131*, 9910–9911.
25. Gomez-Navarro, C.; Meyer, J. C.; Sundaram, R. S.; Chuvilin, A.; Kurasch, S.; Burghard, M.; Kern, K.; Kaiser, U. Atomic Structure of Reduced Graphene Oxide. *Nano Lett.* **2010,** *10*, 1144–1148.
26. Ferrari, A. C.; Robertson, J. Interpretation of Raman Spectra of Disordered and Amorphous Carbon. *Phys. Rev. B* **2000,** *61*, 14095.
27. Ferrari, A. C.; Robertson, J. Resonant Raman Spectroscopy of Disordered, Amorphous, and Diamondlike Carbon. *Phys. Rev. B* **2001,** *64*, 075414.
28. Yang, D.; Velamakanni, A.; Bozoklu, G.; Park, S.; Stoller, M.; Piner, R. D.; Stankovich, S.; Jung, I.; Field, D. A.; Ventrice, C. A., Jr.; Ruoff, R. S. Chemical Analysis of Graphene Oxide Films after Heat and Chemical Treatments by X-ray Photoelectron and Micro-Raman Spectroscopy. *Carbon* **2009,** *47*, 145–152.
29. Kim, S.; Kelley, P. B.; Ortalan, V.; Browning, N. D.; Clifford, A. J. Quality of Graphite Target for Biological/Biomedical/Environmental Applications of ^{14}C-Accelerator Mass Spectrometry. *Anal. Chem.* **2010,** *82*, 2243–2252.
30. Lazzeri, M.; Mauri, F. Nonadiabatic Kohn Anomaly in a Doped Graphene Monolayer. *Phys. Rev. Lett.* **2006,** *97*, 266407.
31. Su, C.; Xu, Y.; Zhang, W.; Zhao, J.; Tang, X.; Tsai, C.; Li, L. Electrical Spectroscopic Characterizations of Ultra-Large Reduced Graphene Oxide Monolayers. *Chem. Mater.* **2009,** *21*, 5647–5680.
32. Becerril, H. A.; Mao, J.; Liu, Z.; Stoltenberg, R. M.; Bao, Z.; Chen, Y. Reduced Graphene Oxide Films as Transparent Conductors. *ACS Nano* **2008,** *2*, 463–470.
33. Shin, H.; Kim, K. K.; Benayad, A.; Yoon, S.; Park, H. K.; Jung, I.; Jin, M. H.; Jeong, H.; Kim, J. M.; Choi, J.; Lee, Y. H. Efficient Reduction of Graphite Oxide by Sodium Borohydride and Its Effect on Electrical Conductance. *Adv. Funct. Mater.* **2009,** *19*, 1987–1992.
34. Fan, X.; Peng, W.; Li, Y.; Li, X.; Wang, S.; Zhang, G.; Zhang, F Deoxygenation of Exfoliated Graphite Oxide under Alkaline Conditions: A Green Route to Graphene Preparation. *Adv. Mater.* **2008,** *20*, 4490–4493.
35. Eda, G.; Fanchini, G.; Chhowalla, M. Large-Area Ultrathin Films of Reduced Graphene Oxide as a Transparent and Flexible Electronic Material. *Nat. Nanotechnol.* **2008,** *3*, 270–274.
36. Li, X.; Zhang, G.; Bai, X.; Sun, X.; Wang, X.; Wang, E.; Dai, H. Highly Conducting Graphene Sheets and Langmuir−Blodgett Films. *Nat. Nanotechnol.* **2008,** *3*, 538–542.
37. Yamaguchi, H.; Eda, G.; Mattevi, C.; Kim, H.; Chhowalla, M. Highly Uniform 300 mm Wafer-Scale Deposition of Single and Multilayered Chemically Derived Graphene Thin Films. *ACS Nano* **2010,** *4*, 524–528.
38. Kim, K. K.; Bae, J. J.; Park, H. K.; Kim, S. M.; Geng, H.; Park, K. A.; Shin, H.; Yoon, S.; Benayad, A.; Choi, J.; Lee, Y. H. Fermi Level Engineering of Single-Walled Carbon Nanotubes by $AuCl_3$ Doping. *J. Am. Chem. Soc.* **2008,** *130*, 12757–12761.